

Charge carrier mobility of halide perovskite single crystals for ionizing radiation detection

Cite as: Appl. Phys. Lett. **119**, 030502 (2021); <https://doi.org/10.1063/5.0057411>

Submitted: 20 May 2021 • Accepted: 01 July 2021 • Published Online: 20 July 2021

 Zheng Zhang and  Bayram Saparov



View Online



Export Citation



CrossMark

ARTICLES YOU MAY BE INTERESTED IN

[Perspective on exchange-coupled quantum-dot spin chains](#)

Applied Physics Letters **119**, 030501 (2021); <https://doi.org/10.1063/5.0055908>

[Unusual defect physics in CH₃NH₃PbI₃ perovskite solar cell absorber](#)

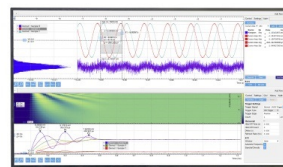
Applied Physics Letters **104**, 063903 (2014); <https://doi.org/10.1063/1.4864778>

[Halide ion migration in lead-free all-inorganic cesium tin perovskites](#)

Applied Physics Letters **119**, 031902 (2021); <https://doi.org/10.1063/5.0054210>

Challenge us.

What are your needs for
periodic signal detection?



Zurich
Instruments



Charge carrier mobility of halide perovskite single crystals for ionizing radiation detection

Cite as: Appl. Phys. Lett. **119**, 030502 (2021); doi: [10.1063/5.0057411](https://doi.org/10.1063/5.0057411)

Submitted: 20 May 2021 · Accepted: 1 July 2021 ·

Published Online: 20 July 2021



View Online



Export Citation



CrossMark

Zheng Zhang and Bayram Saparov^{a)}

AFFILIATIONS

Department of Chemistry and Biochemistry, University of Oklahoma, Norman, Oklahoma 73019-5251, USA

^{a)} Author to whom correspondence should be addressed: saparov@ou.edu

ABSTRACT

Halide perovskites have recently emerged as promising semiconductor materials for several applications including solar cells, light-emitting diodes, and radiation detectors. The charge carrier transport properties, which could be evaluated by the mobility-lifetime ($\mu\tau$ or $\mu\tau$) product, serve an important role for the development of halide perovskites for radiation detection applications. In this Perspective, we first explain the charge transport mechanism and the limiting factors that determine the intrinsic charge carrier mobility in halide perovskite single crystals. Then, we overview the techniques and methods that have been employed for evaluating the charge carrier mobility (for both electrons and holes). Finally, we discuss the discrepancy in the experimentally determined carrier mobility from the literature for halide perovskite single crystals, and provide a perspective on future developments for carrier mobility enhancement.

Published under an exclusive license by AIP Publishing. <https://doi.org/10.1063/5.0057411>

I. INTRODUCTION

Halide perovskites recently attracted much attention due to their outstanding potential in solar cells, photodetectors, and high-energy radiation (x ray/gamma-ray) detectors.^{1–7} The parent halide perovskite has a general formula of ABX_3 , where A is a larger monovalent cation such as methylammonium (MA^+) or formamidinium (FA^+), B is a smaller divalent metal cation such as Pb^{2+} , and X is a halide anion such as Cl^- , Br^- , or I^- . The three-dimensional (3D) crystal structure of the ABX_3 perovskite [Fig. 1(a)] is formed by the corner-sharing $[BX_6]^{4-}$ octahedra with the cubo-octahedral voids filled by relatively small monovalent A cation.⁸ The 3D perovskites, such as $MAPbX_3$, are known to have excellent charge transport properties with high carrier mobility; however, their air/moisture instability and the presence of toxic lead are barriers for their further development into commercial products.^{7,6} For example, $FAPbI_3$ perovskites exposed under ambient air conditions can undergo facile phase transition from α -phase to δ -phase within a few days,⁷ and therefore, are undesirable for long-term use. To resolve the stability and toxicity issues, much effort has been devoted to the manipulations of chemical composition and the crystal structure of perovskites; virtually unlimited materials' design space is available in lower-dimensional perovskite-derived structures including two-dimensional (2D) layered, one-dimensional (1D) chain, and zero-dimensional (0D) cluster halide perovskites, which are formed by excising parts of the inorganic $[BX_3]^-$ framework of the 3D parent perovskite structure.

The 2D layered perovskites constitute large families of $\langle 100 \rangle$ -oriented, $\langle 110 \rangle$ -oriented, and $\langle 111 \rangle$ -oriented perovskites [Fig. 1(b)], each family with its own general chemical formula, as well as more exotic frameworks.^{8–11} Typically, dimensional reduction from the parent 3D perovskite to 2D layered perovskites is achieved through the incorporation of organic cations A' (can be both aromatic or aliphatic) that are too large for the cubo-octahedral A site in the ABX_3 perovskite structure, which results in the “slicing” of the 3D perovskite framework along different crystallographic directions.^{11,12} An important advantage of the low-dimensional perovskites including 2D perovskite is that as the structural dimensionality is reduced, the size restrictions for the components (e.g., as outlined by the tolerance factor) are gradually lifted, providing a much richer compositional phase space for chemical modifications and property fine tuning. On the other hand, the main contributors to the states around the bandgap in the parent lead halide $APbX_3$ perovskites are Pb and X elements, and therefore, the fractioning of the 3D $[PbX_3]$ network into thin 2D layers, 1D chains, or isolated 0D clusters has major influences on the optical and charge transport properties of the resultant materials. Thus, 2D perovskites typically not only have much poorer and anisotropic charge transport properties but also exhibit much more enhanced moisture stability owing to the protective organic cationic layers in between the inorganic perovskite layers [Fig. 1(b)].^{13,14} In most 2D layered perovskites, charge carriers are limited to be effectively transported only along the inorganic perovskite layers.⁸ Similar to 2D perovskites, 1D

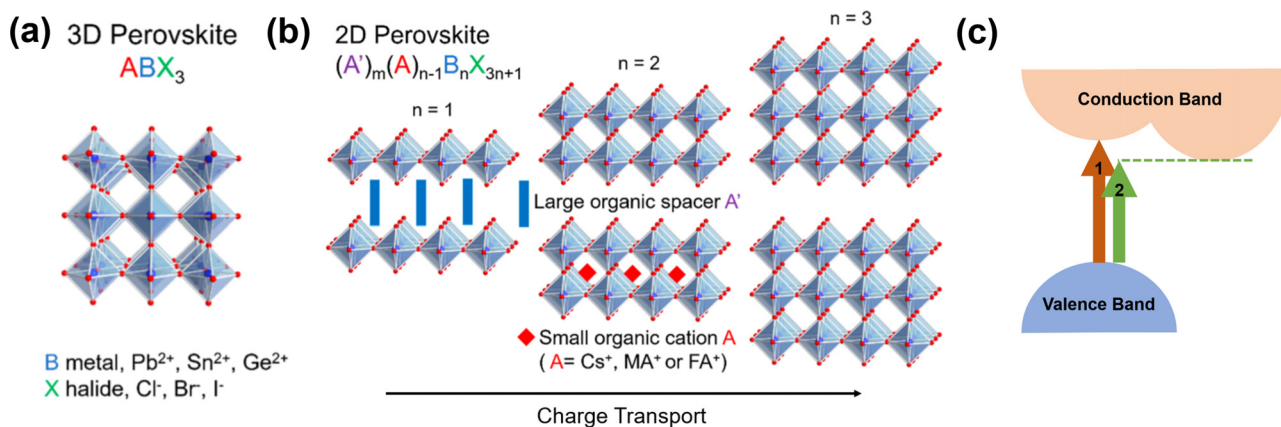


FIG. 1. Crystal structures of (a) the parent 3D ABX_3 perovskite and (b) its layered 2D perovskite derivative. [Reproduced with permission from Mao *et al.*, J. Am. Chem. Soc. **141**, 1171 (2019).²¹ Copyright 2019 American Chemical Society.] (c) Illustration of the direct (1) and indirect (2) band-to-band transitions for perovskite semiconductors.

perovskites feature chains made of corner sharing of $[BX_6]^{4-}$ octahedra that are isolated in two dimensions by the A cations separating the chains. However, we note that although the parent 3D perovskite structure features only corner sharing of the $[BX_6]^{4-}$ octahedra, in recent years, the halide perovskites terminology has been loosely applied to all kinds of metal halide networks including various units formed by corner-sharing, edge-sharing, and face-sharing arrangements.¹⁵ In 0D perovskites, each individual metal halide octahedral cluster is completely isolated and surrounded by organic cations, and thus, 0D perovskites usually possess the poorest charge transport properties.

The development of halide perovskites in their single crystals' form for ionizing radiation detection has witnessed a rapid growth over the past few years. In 2013, Stoumpos *et al.* studied the optoelectronic properties of $CsPbBr_3$ semiconductors for high-energy radiation detection; however, no energy-resolving performance was reported in this work.¹⁶ In 2016, Dirin *et al.* for the first time showed that the same material could respond to 59.5 keV gamma-rays.¹⁷ Another 3D perovskite, $FAPbI_3$, also has been reported as effective material for gamma photon detection.¹⁸ More recently, He *et al.* demonstrated that $CsPbBr_3$ could be used for wide range gamma-ray detection with superior energy resolution.¹⁹ Such remarkable progress of halide perovskites within such a short development period clearly shows the strong potential of this material class for the use in the next-generation room temperature radiation detectors. Despite early success and great potential of halide perovskites, accurate characterization of the charge transport of this remarkably diverse material class is still a work in progress.²⁰ Among the important issues are the facts that their charge carrier transport is not well understood, and there is a large variation in the reported mobility values in the literature. In this Perspective, we overview the charge transport mechanisms in halide perovskites and discuss the discrepancy and variance between the reported experimentally determined carrier mobilities with a major focus on the prospective use of halide perovskites for radiation detection. A prospect on element doping for enhancing the intrinsic carrier density of halide perovskites is provided.

II. CHARGE TRANSPORT MECHANISM

Charge carrier mobility μ is the drift velocity v of charge carriers per unit of electric field E . Therefore, mobility is expressed using the below formula:

$$\mu = \frac{v}{E}. \quad (1)$$

In intrinsic semiconductors, charge carrier electrons are sitting in the valence band [Fig. 1(c)] and unable to move freely to conduct the current flow. By heat or photon excitations, charge carriers could gain enough energy to move to the conduction band, and therefore, become free electrons. The empirical formula of electron-hole pair creation energy W (eV) that is applicable for halide perovskites is²²

$$W = 2E_g + 1.43, \quad (2)$$

where E_g is the bandgap energy from the valence band maximum (VBM) to the conduction bandgap minimum (CBM). The valence-to-conduction band transitions could be either direct-type [marked by the orange arrow in Fig. 1(c)] or indirect-type [marked by the green arrow in Fig. 1(c)]; the nature of the optical bandgap determines if the phonon participation for electron momentum conservation is necessary.

Charge carrier mobility of perovskite semiconductors is a complex parameter that is influenced by temperatures, crystal structures, carrier concentrations, and doping levels. Yi *et al.* reported the temperature-dependent Hall mobility for $MAPbBr_3$ single crystals across the cubic-to-tetragonal phase transition [Fig. 2(a)]. The results suggest that acoustic-phonon and space-charge carrier scattering mechanisms may dominate, respectively, in the two different $MAPbBr_3$ crystal structures. The impurity dopants could serve as either donors or acceptors to modify the carrier mobility. The donor impurity "donate" electrons to the perovskite hosts, reversed situation suits the acceptors. Figure 2(b) shows the measured Hall mobility for as-grown and Sn^{IV} -doped tin perovskite $MASnI_3$ single crystals. Material defects are also playing an important role for the charge transport, and therefore, are directly linked to the charge transport mechanism. Electrons could be trapped by deep-level vacancy-type defects, and thus, could not be effectively transported toward the conduction band. Dislocation-type defects could enhance the scattering probability of electrons. To enhance the carrier mobility and charge transport properties, suppressing the formation of deep-level defects plays a vital role. In some scenarios, this may be simply achieved by adjusting the loading ratio of starting chemicals for the subsequent

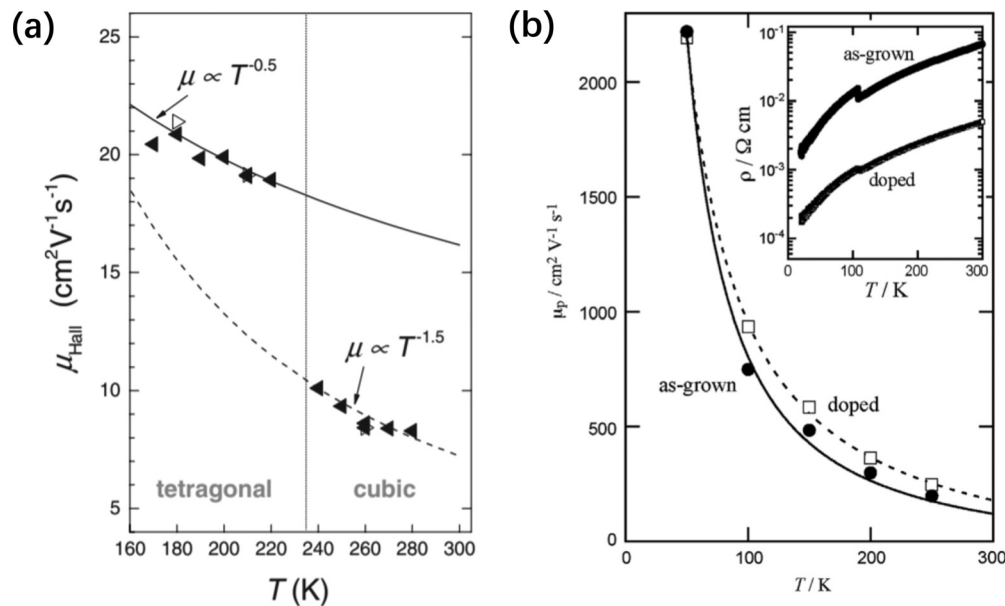


FIG. 2. (a) Temperature dependence on the Hall mobility for MAPbBr₃ single crystals. [Reproduced with permission from Yi *et al.*, Adv. Mater. **28**, 6509 (2016).²³ Copyright 2016 John Wiley and Sons.] (b) Determined Hall mobility for as-grown and artificially Sn^{IV}-doped MASnI₃ single crystals. [Reproduced with permission from Takahashi *et al.*, J. Solid State Chem. **205**, 39 (2013).²⁴ Copyright 2013 Elsevier Inc.]

solution-processing of halide perovskites. Theoretical reports suggest that Cs₂AgBiBr₆ double perovskites could be grown from Bi-poor/Br-rich solutions to suppress the formation of deep-level vacancy and anti-substitution defects V_{Br} and Bi_{Ag}.²⁵ Optimized crystal growth and compositional engineering using cation/halide substitutions could be key solutions for controlling the concentration of deep-level defects.²⁶

III. MEASUREMENT METHODS AND TECHNIQUES

A. Time-of-flight

The time-of-flight (ToF) technique measures the velocity of charge carriers under a certain applied electric field. The charge carrier velocity v (cm/s) can be simply determined using $v = L/t$, where L (cm) is the carrier drift distance and t (s) is the carrier drift time. To evaluate the carrier mobility of halide perovskites, a single crystal-based device is usually fabricated with metal electrodes deposited on the two opposite sides of a thick single crystal. Charge carriers are then produced by heat/photon excitations and being pulled toward cathodes (holes) and anodes (electrons) if a certain bias voltage is applied [Fig. 3(a)]. In the scenario that charge carriers are being produced on the device surface and could travel the entire distance between the two opposite electrodes, the carrier drift distance L then equals the length between the two opposite electrodes. To determine the carrier velocity, the carrier drift time could be determined from the ToF pulse trace. Figure 3(b) shows the ToF pulse trace using a TlSn₂I₅ perovskite-based detector,²⁷ which was excited by the Am-241 alpha source. The carrier drift time (or transit time) is then read as two times the time it requires for the voltage amplitude to reach half of the maximum, or it could be read as the time takes from 10% to 90% of the maximum amplitude. It should be noted that the ToF technique is device-oriented and very useful for separately determining the hole mobility and the electron mobility.

B. Space-charge-limited-current

Space-charge-limited-current (SCLC) is another technique that has been widely employed for determining the charge carrier mobility. In SCLC measurements, there are three transition regimes: Ohmic, trap-filled limited (TFL), and child. Figures 3(c) and 3(d) show the SCLC measurement results for MAPbBr₃ and MAPbI₃ perovskite single crystals. The charge carrier mobility is evaluated from the child regime (a trap-free region), where the injected charge carriers from metal contacts dominate over the intrinsic charge carriers in halide perovskites, and thus, the charge carrier mobility is no longer a function of intrinsic charge carrier concentration. Owing to such, the SCLC technique is typically more accurate for determining the carrier mobility as compared to the ToF method. In the child regime of a SCLC curve, the carrier mobility μ is evaluated using the Mott–Gurney law²⁹

$$\mu = \frac{8J_D L^3}{9\epsilon\epsilon_0 V^2}, \quad (3)$$

where J_D is the current density, ϵ is the dielectric constant, ϵ_0 is the vacuum permittivity, and L is the crystal thickness.

C. Hall effect

Hall effect is a measure of the charge carrier behaviors under both the electrical and magnetic fields. When the magnetic field acts perpendicularly to the current flow direction in perovskite single crystals, a Lorentz force that is in the direction transverse to the current flow is produced. Under the Lorentz force, the charge carrier moving direction is deflected. Holes and electrons are deflected to opposite directions owing to the positive charge of holes and the negative charge of electrons. The positive or negative sign of the Hall voltage

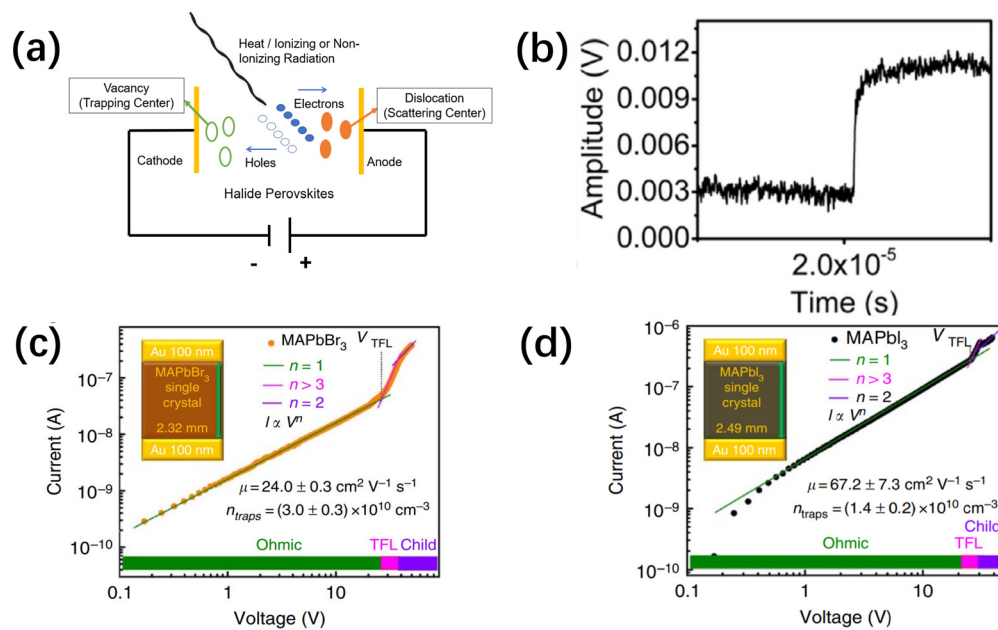


FIG. 3. (a) Illustration of the working principle of halide perovskite semiconductor-based radiation detectors and the effect of vacancy and dislocation type defects for charge transport. (b) ToF pulse signal using the TiSn_2I_5 perovskite-based detector, excited by an Am-241 alpha source. [Reproduced with permission from Lin *et al.*, ACS Photonics **4**, 1805 (2017).²⁷ Copyright 2017 American Chemical Society.] (c) and (d) SCLC curves with marked Ohmic, TFL, and child regimes for MAPbBr_3 and MAPbI_3 perovskite single crystals. [Reproduced with permission from Saidaminov *et al.*, Nat. Commun. **6**, 23955 (2015).²⁸ Copyright Springer Nature 2015.]

V_H , therefore, could be used to determine the conduction type (p or n) of halide perovskite semiconductor solids. Carrier mobility could be evaluated from Hall effect measurement using

$$\mu = \frac{R_H}{\rho}, \quad (4)$$

where R_H is the Hall coefficient and ρ is the semiconductor resistivity.

D. Time-resolved terahertz spectroscopy and time-resolved microwave conductivity

Time-resolved terahertz spectroscopy (TRTS) is a contactless ultrafast probe technique that is widely used for thin film studies and employs visible excitations to acquire the transient photoconductivity from specimens. It can be done using either transmission or reflection mode. For halide perovskite single crystals, the measurement is very challenging in the transmission mode, which requires the specimen to be transparent. Few reports have been made with this technique to study the carrier mobility of halide perovskite single crystal specimens.^{30,31} A similar contactless measurement technique is time-resolved microwave conductivity (TRMC), which essentially monitors the transient change in microwave reflectivity that charge carriers produce after the sample has been photoexcited by a nanosecond laser pulse.³² Using the TRMC method, the relative change of microwave power that relates to the charge carrier mobility could be measured and expressed below:^{33,34}

$$\frac{\Delta P(t)}{P} = Ae \sum_i \Delta n_i(t) \mu_i = Ae (\Delta n_e(t) \mu_e + \Delta n_h(t) \mu_h), \quad (5)$$

where A is a microwave frequency-dependent sensitivity factor, μ_e and μ_h are electron and hole mobilities, respectively, and n_e and n_h are the electron and hole concentrations. It should be, however, noted that TRTS and TRMC techniques cannot distinguish the electron and hole contributions, and the extracted parameter is a sum of electron and hole mobilities.

E. Suitability of the measurement techniques

As discussed above, the ToF drift mobility is device-oriented, and therefore, is very useful for device characterizations. Nevertheless, to determine the carrier mobility using the ToF technique, the sample thickness has to be suitable for ToF evaluation. This is because the carrier drift length λ ($\lambda = \mu \tau E$, where E is the electric field) is limited by the carrier mobility-lifetime product and the applied electric field. SCLC is also a device-based technique; however, the carrier mobility determined using the SCLC technique is no longer a function of intrinsic carrier concentration, and therefore, is more accurate than the ToF drift mobility. The Hall mobility is slightly different from the carrier drift mobility, which originates from the different charge transport scattering mechanisms (e.g., ionized-impurity scattering, charged dislocation scattering, and lattice scattering) under both the electrical and magnetic fields. For example, the Hall mobilities determined for single crystal silicon are 1560 and 345 $\text{cm}^2/\text{V s}$ for electrons and holes, whereas the drift mobility values are 1360 and 510 $\text{cm}^2/\text{V s}$, respectively.³⁵ In addition, under low electrical field conditions, charge carriers mainly undergo Coulomb and phonon scattering as they are almost in equilibrium with lattice vibrations.³⁶ Under high electrical field conditions, the carrier mobility becomes a field-dependent parameter. The Coulomb scattering dominates over the phonon

scattering at low temperatures; however, Coulomb scattering and phonon scattering compete at high temperatures due to the lattice vibrations.³⁷ Theoretical models also have been proposed to predict the carrier mobility as a function of electrical field and temperatures.³⁸ In contrast to the ToF and SCLC measurement techniques that require contacts, TRMC and TRTS take the precedence when high-quality electrode contacts are not accessible. Metal contacts with poor-quality could lead to band bending and contact resistance. In SCLC experiments, poor-quality electrode contacts could even lead the trap-independent child regime to be difficult to reach for reliable mobility retraction. However, the TRTS measurement is complicated for thick single crystal samples and could not yield the mobility for holes and electrons as the ToF technique.

It also should be noted that the field-effect transistor (FET) method has been used to determine the carrier mobility of halide perovskites.^{39,40} Essentially, the carrier mobility could be derived from the saturation regime using the relationship between I_{DS} (drain current) and V_{GS} (gate voltage) described as below:^{39,41}

$$I_{DS} = \frac{W}{2L} C_i \mu (V_{GS} - V_{TH})^2, \quad (6)$$

where W and L are the channel width and length, respectively. C_i is the capacitance of the gate electrode, and V_{TH} is the threshold voltage. The FET method is sensitive to the device fabrication conditions (e.g., temperature, perovskite surface morphology, grain size, and electrode materials)³⁹ and more suitable for evaluating the thin-film device-based carrier mobility of halide perovskites toward transistor applications.

IV. MEASUREMENT DISCREPANCY AND FUNDAMENTAL LIMITS

In polycrystalline perovskite thin films, charge transport is typically limited compared to single crystals due to the grain boundaries, and thus, carrier mobilities for thin films are usually orders of magnitude lower in contrast to that for single crystals. However, it also needs to be mentioned that the local techniques TRTS and TRMC, which are generally adopted for determining the thin film carrier mobilities, are less likely affected by the grain boundaries. For example, MAPbI₃ perovskite thin film carrier mobility is 35 cm²/V s as determined by terahertz spectroscopy,⁴² whereas the MAPbI₃ single crystal carrier mobility is 65 ± 6 cm²/V s as measured by SCLC.⁴⁸ The reported carrier mobility values of electrons and holes for halide perovskites single crystals are summarized in Table I. As expected from the structural considerations, 3D perovskites, such as MAPbI₃ and CsPbBr₃, exhibit relatively high charge carrier mobilities; however, the reported carrier mobilities are noticeably different. There is a vast range for the reported mobilities even for the same perovskite structure and chemical composition. For example, the reported mobility values range from 4.4 to 150 ± 15 cm²/V s for the single crystals of FAPbI₃.^{7,46–48} Similar situation applies to FAPbBr₃, the experimentally determined mobility values surprisingly could have two orders of magnitude difference. Such large discrepancy in the experimentally measured carrier mobilities could be related to the determination of the child regime from the SCLC curve. In the child regime, current (I) is proportional to the square of the voltage (V^2). It is necessary to ensure the child regime is fitted accurately to extract the reliable proportional constant from this region. In fact, as proposed recently by Le Corre *et al.*,⁴⁹ the traditional manner of using SCLC for studying halide perovskites may need to be

TABLE I. Summary of the experimentally determined charge carrier mobility for halide perovskite single crystals. Unless otherwise mentioned, the carrier mobility is measured at room temperature (h: hole and e: electron) (DABCO is N-N'-diazabicyclo[2.2.2]octonium).

Perovskite	Mobility (cm ² /V s)	Method	Reference
Three-dimensional (3D) perovskites			
MAPbI ₃	105 ± 35 (h)	Hall	29
	164 ± 25 (h)	SCLC	
	24.0 ± 6.8 (e)	ToF	
	65 ± 6	SCLC	48
	60	TRTS	30
	620	TRTS	31
	35	TRTS	77
	130 ± 20 (n-Type)	TRMS	78
MASnI ₃	42 ± 5 (p-Type)		
	2320 (e)	Hall	53
	322 (h)		
MAPbBr ₃	200 (at 250 K)	Hall	24
	35 ± 2 (h)	SCLC	65
	24.0	SCLC	28
MAPbCl ₃	42 ± 9	SCLC	66
FAPbI ₃	4.4	SCLC	7
	35 ± 7	SCLC	46
	40 ± 5	SCLC	47
	150 ± 15	SCLC	48
	62 ± 11 (h)	SCLC	46
FAPbBr ₃	0.12	SCLC	67
FAPbBr _{2.23} Cl _{0.77}	12	SCLC	67
FAPb _{0.97} Sn _{0.03} Br ₃	0.22	SCLC	67
MA _{0.45} FA _{0.55} PbI ₃	271 ± 60	SCLC	48
CsPbBr ₃	181 (e)	ToF	68
	56.5 (h)		
	63 (e)	ToF	51
	49 (h)		
	1.78 (h)	ToF	50
CsPbCl ₃	9.71–38.5	Hall	69
	28 ± 1 (e)	ToF	70
	20 ± 1 (h)		
FA _{0.9} Cs _{0.05} MA _{0.05}	197 (e)	SCLC	71
PbI _{2.7} Br _{0.3}	219 ± 18 (h)		
Cs ₂ AgBiBr ₆	7.02	SCLC	4
	3.17	SCLC	43
	5	ToF	44
Two-dimensional (2D) perovskites			
MA ₃ Sb ₂ I ₉	16.68	SCLC	64
Sn-doped MA ₃ Sb ₂ I ₉	43.05	SCLC	64
Rb ₃ Sb ₂ I ₉	0.32 (e)	ToF	72
Cs ₃ Sb ₂ I ₉	0.14 (h)	ToF	72
(NH ₄) ₃ Bi ₂ I ₉	213	SCLC	75
PEA ₂ MA ₂ Pb ₃ I ₁₀	4.4 × 10 ⁻²	SCLC	84
One-dimensional (1D) perovskites			
(DME)PbBr ₄	>4.51	SCLC	52

TABLE I. (Continued.)

Perovskite	Mobility ($\text{cm}^2/\text{V s}$)	Method	Reference
Zero-dimensional (0D) perovskites			
$\text{Cs}_3\text{Bi}_2\text{I}_9$	4.3 (e) 1.7 (h)	ToF	72
$\text{FA}_3\text{Bi}_2\text{I}_9$	4	Hall	73
$\text{MA}_3\text{Bi}_2\text{I}_9$	70 1–6 (h) 2–8 (e)	Hall ToF	74
Metal-free perovskites			
$\text{DABCO-NH}_4\text{Br}_3$	2.00 (h) 0.67 (e) 2.08	SCLC Hall	45

entirely revisited. The vast disagreement may be explained by the fact that SCLC consistently leads to over- or under-estimation of the charge carrier mobility as the influence of ionic species in halide perovskites is simply neglected when such measurements are performed. Instead, a pulsed SCLC is suggested as the ion species do not have sufficient time to migrate and shield the charge from the traps in such measurements.⁴⁹ On the other hand, experimental variations also should be partially blamed for such discrepancy. For CsPbBr_3 , the reported hole mobility by Pan *et al.* using the ToF technique is $1.78 \text{ cm}^2/\text{V s}$.⁵⁰ He *et al.* reported that the hole mobility is $49 \text{ cm}^2/\text{V s}$.⁵¹ In this case, the discrepancy is likely due to the different crystal growth methods (Bridgman melt and solution growth, respectively) employed for producing single crystals, which then lead to crystal quality variations.

One popular class among the lower-dimensional family is $\text{A}_3\text{B}_2\text{X}_9$ perovskites, which have either 2D or 0D crystal structure. Their mobility is typically one order magnitude lower as contrast to 3D ones. However, $(\text{NH}_4)_3\text{Bi}_2\text{I}_9$ surprisingly has a high carrier mobility of $213 \text{ cm}^2/\text{V s}$ measured by SCLC, implying that even though 2D halide perovskite may have poorer charge transport properties, they should not be neglected and may even outperform the parent 3D perovskites. The mobility for one-dimensional $(\text{DME})\text{PbBr}_4$ is $4.51 \text{ cm}^2/\text{V s}$,⁵² which is as expected much poorer than that for MASnI_3 and MAPbI_3 .^{29,53} Nevertheless, low-dimensional perovskites have been demonstrated to have suppressed ionic migration with better long-term operation stability.^{54,55} Therefore, low-dimensional ones and even the recent arising metal-free halide perovskites may be able to serve as new promising candidates to replace the 3D lead halide perovskites for high sensitivity x-ray detection.

Based on the literature reported values, it is noticeable that very few perovskite single crystals have carrier mobilities exceeding $300 \text{ cm}^2/\text{V s}$, which is much lower than that for conventional inorganic semiconductors GaAs ($9400 \text{ cm}^2/\text{V s}$ for electrons), GaN ($1000 \text{ cm}^2/\text{V s}$ for electrons), and cadmium zinc telluride (CdZnTe , $1373 \text{ cm}^2/\text{V s}$ for electrons) for ionizing radiation detection.^{56–59} The charge carrier mobility limitations for halide perovskites have been attributed to mechanisms such as strong electron–phonon coupling, which leads to the formation of polarons, and thus, enhanced effective mass of charge carriers.^{60,61} However, the formation of polarons

remains an open question requiring further studies. Another possible explanation is the highly insulating nature of halide perovskites.⁵⁷ Halide perovskites have been known to exhibit very high resistivities ($>10^7 \Omega \text{ cm}$) with low electronic conductivity and carrier density, thus measuring Hall mobility for halide perovskites is typically very challenging. As carrier mobility is highly dependent on carrier density, enhancing the carrier density becomes the key for extracting the intrinsic carrier mobility of halide perovskites. Several reports have shown that the AC photo-Hall technique is able to reveal the intrinsic carrier mobility of halide perovskites at a high carrier density regime, enabling simultaneously extracting mobilities for majority and minority charge carriers meanwhile with the carrier-resolving capability.^{57,62} Meanwhile, a recent report suggests that doping MAPbI_3 thin films with sodium could turn MAPbI_3 into highly conductive p-type semiconductors and, thus, enhance the hole carrier concentration.⁶³ Similar doping strategy should be applicable for other halide perovskite single crystals, as demonstrated by a recent example of Sn-doped $\text{MA}_3\text{Sb}_2\text{I}_9$.⁶⁴

V. SUMMARY AND CONCLUSIONS

Halide perovskites-based radiation detectors have shown encouraging energy-resolving performance with the added benefit of low material cost from solution processing. These advantageous characteristics distinguish perovskite single crystals as promising alternatives to the leading semiconductor detector materials such as CdZnTe . Importantly, this field is still in its infancy, and the carrier mobility of halide perovskites could be further enhanced, e.g., by elemental doping and cation engineering methods, to accelerate their development for wide commercial deployment. Specifically, more beneficial work can be done to dope halide perovskites (especially the iodide version of 3D perovskites that have suitable bandgap energy E_g) with the aim of enhancing their intrinsic carrier density. On the A cation site, a few recent reports attempted to elucidate the role that organic cations play for varying the charge carrier dynamics in halide perovskites.^{79,80} Though the findings remain under debate, the fact that the organic cations can play a pivotal role in the optoelectronic properties of hybrid materials has been evidenced in a number of low-dimensional metal halides.^{11,81,82} Therefore, further exploration of employing different organic cations to tune the material's optical bandgap and the orbital makeup of states around the optical bandgap is warranted. Low highest occupied molecular orbital (HOMO) and lowest unoccupied molecular orbital (LUMO) gap π -conjugated organic species with relatively high dielectric constant may be the ultimate solution to break the dielectric confinement “bottleneck” in low-dimensional perovskites.⁸³ On the B-site front, tin(II) perovskites exhibit superior charge transport properties in the perovskite family, which makes them stand out. However, instability of Sn(II) perovskites due to the facile oxidation of Sn^{2+} to Sn^{4+} remains to be a significant challenge requiring further research. A further key challenge in the field is the vastly different carrier mobilities reported in the literature for the same perovskite composition and stoichiometry. Newly developed techniques, such as the AC photo-Hall measurements, may provide more accurate data for halide perovskites. In addition, dislocation related carrier scattering in halide perovskites may be reduced by suitably altering the crystal synthesis conditions. Density functional theory (DFT) and *ab initio* calculations also have been widely used to study halide perovskites and predict their charge transport properties.^{85–87} However, the

development of an accurate theoretical model for fully elucidating the charge carrier dynamics in halide perovskites is still a challenging problem. For example, the slow migration of halide ion species, which plays a vital role for the charge carrier transport, could not yet be simulated. It is necessary for a theoretical model to consider the lattice fluctuations, halide ion diffusion, and the electron–phonon coupling. In combination with the experimental verifications, accurate modeling of the charge transport and chemical dynamics of halide perovskites will aid the development of halide perovskites for optoelectronic applications.

ACKNOWLEDGMENTS

This material was based upon the work supported by the U.S. Department of Energy, Office of Science, Office of Basic Energy Sciences, under Award No. DE-SC0021158.

This report was prepared as an account of work sponsored by an agency of the United States Government. Neither the United States Government nor any agency thereof, nor any of their employees, makes any warranty, express or implied, or assumes any legal liability or responsibility for the accuracy, completeness, or usefulness of any information, apparatus, product, or process disclosed, or represents that its use would not infringe privately owned 12 rights. Reference herein to any specific commercial product, process, or service by trade name, trademark, manufacturer, or otherwise does not necessarily constitute or imply its endorsement, recommendation, or favoring by the United States Government or any agency thereof. The views and opinions of authors expressed herein do not necessarily state or reflect those of the United States Government or any agency FA R&D Special TC November 2017–FF Page 4 of 12 thereof.

DATA AVAILABILITY

Data sharing is not applicable to this article as no new data were created or analyzed in this study.

REFERENCES

- P. Tonui, S. O. Oseni, G. Sharma, Q. Yan, and G. Tessema Mola, *Renewable Sustainable Energy Rev.* **91**, 1025 (2018).
- J. Miao and F. Zhang, *J. Mater. Chem. C* **7**, 1741 (2019).
- H. Mescher, F. Schackmar, H. Eggers, T. Abzieher, M. Zuber, E. Hamann, T. Baumbach, B. S. Richards, G. Hernandez-Sosa, U. W. Paetzold, and U. Lemmer, *ACS Appl. Mater. Interfaces* **12**, 15774 (2020).
- Z. Zhang, C. C. Chung, Z. Huang, E. Vetter, D. Seyitliyev, D. Sun, K. Gundogdu, F. N. Castellano, E. O. Danilov, and G. Yang, *Mater. Lett.* **269**, 127667 (2020).
- X. Li, C. Meng, B. Huang, D. Yang, X. Xu, and H. Zeng, *Adv. Opt. Mater.* **8**, 2000273 (2020).
- Z. Zhang and G. Yang, *J. Mater. Sci. Mater. Electron.* **1**, 3 (2020).
- Q. Han, S. H. Bae, P. Sun, Y. T. Hsieh, Y. Yang, Y. S. Rim, H. Zhao, Q. Chen, W. Shi, G. Li, and Y. Yeng, *Adv. Mater.* **28**, 2253 (2016).
- G. Grancini and M. K. Nazeeruddin, *Nat. Rev. Mater.* **4**, 4 (2019).
- D. H. Cao, C. C. Stoumpos, O. K. Farha, J. T. Hupp, and M. G. Kanatzidis, *J. Am. Chem. Soc.* **137**, 7843 (2015).
- C. C. Stoumpos, D. H. Cao, D. J. Clark, J. Young, J. M. Rondinelli, J. I. Jang, J. T. Hupp, and M. G. Kanatzidis, *Chem. Mater.* **28**, 2852 (2016).
- B. Saparov and D. B. Mitzi, *Chem. Rev.* **116**, 4558 (2016).
- A. L. Abdelhady and M. I. Saidaminov, *Chem* **5**, 2513 (2019).
- G. Grancini, C. Roldán-Carmona, I. Zimmermann, E. Mosconi, X. Lee, D. Martineau, S. Narbey, F. Oswald, F. de Angelis, M. Graetzel, and M. K. Nazeeruddin, *Nat. Commun.* **8**, 15684 (2017).
- H. Tsai, W. Nie, J. C. Blancon, C. C. Stoumpos, R. Asadpour, B. Harutyunyan, A. J. Neukirch, R. Verduzco, J. J. Crochet, S. Tretiak, L. Pedesseau, J. Even, M. A. Alam, G. Gupta, J. Lou, P. M. Ajayan, M. J. Bedzyk, M. G. Kanatzidis, and A. D. Mohite, *Nature* **536**, 312 (2016).
- H. Lin, C. Zhou, Y. Tian, T. Siegrist, and B. Ma, *ACS Energy Lett.* **3**, 54 (2018).
- C. C. Stoumpos, C. D. Malliakas, J. A. Peters, Z. Liu, M. Sebastian, J. Im, T. C. Chasapis, A. C. Wibowo, D. Y. Chung, A. J. Freeman, B. W. Wessels, and M. G. Kanatzidis, *Cryst. Growth Des.* **13**, 2722 (2013).
- D. N. Dirin, I. Cherniukh, S. Yakunin, Y. Shynkarenko, and M. V. Kovalenko, *Chem. Mater.* **28**, 8470 (2016).
- S. Yakunin, D. N. Dirin, Y. Shynkarenko, V. Morad, I. Cherniukh, O. Nazarenko, D. Kreil, T. Nauser, and M. V. Kovalenko, *Nat. Photonics* **10**, 585 (2016).
- Y. He, L. Matei, H. J. Jung, K. M. McCall, M. Chen, C. C. Stoumpos, Z. Liu, J. A. Peters, D. Y. Chung, B. W. Wessels, M. R. Wasielewski, V. P. Dravid, A. Burger, and M. G. Kanatzidis, *Nat. Commun.* **9**, 4383 (2018).
- L. M. Herz, *Annu. Rev. Phys. Chem.* **67**, 65 (2016).
- L. Mao, C. C. Stoumpos, and M. G. Kanatzidis, *J. Am. Chem. Soc.* **141**, 1171 (2019).
- R. Devanathan, L. R. Corrales, F. Gao, and W. J. Weber, *Nucl. Instrum. Methods Phys. Res., Sect. A* **565**, 637 (2006).
- H. T. Yi, X. Wu, X. Zhu, and V. Podzorov, *Adv. Mater.* **28**, 6509 (2016).
- Y. Takahashi, H. Hasegawa, Y. Takahashi, and T. Inabe, *J. Solid State Chem.* **205**, 39 (2013).
- T. Li, X. Zhao, D. Yang, M. H. Du, and L. Zhang, *Phys. Rev. Appl.* **10**, 041001 (2018).
- R. Brakkee and R. M. Williams, *Appl. Sci.* **10**, 3061 (2020).
- W. Lin, C. C. Stoumpos, Z. Liu, S. Das, O. Y. Kontsevoi, Y. He, C. D. Malliakas, H. Chen, B. W. Wessels, and M. G. Kanatzidis, *ACS Photonics* **4**, 1805 (2017).
- M. I. Saidaminov, A. L. Abdelhady, B. Murali, E. Alarousu, V. M. Burlakov, W. Peng, I. Dursun, L. Wang, Y. He, G. MacUlán, A. Goriely, T. Wu, O. F. Mohammed, and O. M. Bakr, *Nat. Commun.* **6**, 23955 (2015).
- Q. Dong, Y. Fang, Y. Shao, P. Mulligan, J. Qiu, L. Cao, and J. Huang, *Science* **347**, 967 (2015).
- C. Q. Xia, Q. Lin, J. B. Patel, A. D. Wright, T. W. Crothers, R. L. Milot, L. M. Herz, and M. B. Johnston, in *International Conference on Infrared, Millimeter, and Terahertz Waves, IRMMW-THz* (IEEE Computer Society, 2019).
- D. A. Valverde-Chávez, C. S. Ponseca, C. C. Stoumpos, A. Yartsev, M. G. Kanatzidis, V. Sundström, and D. G. Cooke, *Energy Environ. Sci.* **8**, 3700 (2015).
- R. Brenot, R. Vanderhaghen, B. Drevillon, I. French, P. Roca, and I. Cabarrocas, *Thin Solid Films* **296**, 94 (1997).
- J. Peng, Y. Chen, K. Zheng, T. Pullerits, and Z. Liang, *Chem. Soc. Rev.* **46**, 5714 (2017).
- C. Colbeau-Justin and M. A. Valenzuela, *Rev. Mex. Fis.* **59**, 191 (2013).
- D. C. Cronemeyer, *Phys. Rev.* **105**, 522 (1957).
- D. K. Schroder, *Advanced Mos Devices (Modular Series on Solid State Devices)* (Addison-Wesley, Boston, 1987).
- C. Hu, S. Khandelwal, Y. S. Chauhan, T. McKay, J. Watts, J. P. Duarte, P. Kushwaha, and H. Agarwal, *Industry Standard FDSOI Compact Model BSIM-IMG for IC Design* (Woodhead Publishing, 2019), Vol. 1.
- K. Alfaramawi, *Bull. Mater. Sci.* **37**, 1603 (2014).
- W. Yu, F. Li, L. Yu, M. R. Niazi, Y. Zou, D. Corzo, A. Basu, C. Ma, S. Dey, M. L. Tietze, U. Buttner, X. Wang, Z. Wang, M. N. Hedhili, C. Guo, T. Wu, and A. Amassian, *Nat. Commun.* **9**, 23955 (2018).
- J. Wang, S. P. Senanayak, J. Liu, Y. Hu, Y. Shi, Z. Li, C. Zhang, B. Yang, L. Jiang, D. Di, A. V. Ievlev, O. S. Ovchinnikova, T. Ding, H. Deng, L. Tang, Y. Guo, J. Wang, K. Xiao, D. Venkateshvaran, L. Jiang, D. Zhu, and H. Sirringhaus, *Adv. Mater.* **31**, 1902618 (2019).
- T. Matsushima, M. R. Leyden, T. Fujihara, C. Qin, A. S. D. Sandanayaka, and C. Adachi, *Appl. Phys. Lett.* **115**, 120601 (2019).
- R. L. Milot, G. E. Eperon, H. J. Snaith, M. B. Johnston, and L. M. Herz, *Adv. Funct. Mater.* **25**, 6218 (2015).
- W. Pan, H. Wu, J. Luo, Z. Deng, C. Ge, C. Chen, X. Jiang, W. J. Yin, G. Niu, L. Zhu, L. Yin, Y. Zhou, Q. Xie, X. Ke, M. Sui, and J. Tang, *Nat. Photonics* **11**, 726 (2017).

- ⁴⁴Z. Zhang, D. Cao, Z. Huang, E. O. Danilov, C. C. Chung, D. Sun, and G. Yang, *Adv. Opt. Mater.* **9**, 2001575 (2021).
- ⁴⁵X. Song, Q. Cui, Y. Liu, Z. Xu, H. Cohen, C. Ma, Y. Fan, Y. Zhang, H. Ye, Z. Peng, R. Li, Y. Chen, J. Wang, H. Sun, Z. Yang, Z. Liu, Z. Yang, W. Huang, G. Hodes, S. Liu, and K. Zhao, *Adv. Mater.* **32**, 2003353 (2020).
- ⁴⁶A. A. Zhumekenov, M. I. Saidaminov, M. A. Haque, E. Alarousu, S. P. Sarmah, B. Murali, I. Dursun, X. H. Miao, A. L. Abdelhady, T. Wu, O. F. Mohammed, and O. M. Bakr, *ACS Energy Lett.* **1**, 32 (2016).
- ⁴⁷Y. Liu, J. Sun, Z. Yang, D. Yang, X. Ren, H. Xu, Z. Yang, and S. F. Liu, *Adv. Opt. Mater.* **4**, 1829 (2016).
- ⁴⁸W. G. Li, H. S. Rao, B. X. Chen, X. D. Wang, and D. Bin Kuang, *J. Mater. Chem. A* **5**, 19431 (2017).
- ⁴⁹V. M. Le Corre, E. A. Duijnste, O. E. Tambouli, J. M. Ball, H. J. Snaith, J. Lim, and L. J. A. Koster, *ACS Energy Lett.* **6**, 1087 (2021).
- ⁵⁰L. Pan, Y. Feng, J. Huang, and L. R. Cao, *IEEE Trans. Nucl. Sci.* **67**, 2255 (2020).
- ⁵¹Y. He, Z. Liu, K. M. McCall, W. Lin, D. Y. Chung, B. W. Wessels, and M. G. Kanatzidis, *Nucl. Instrum. Methods Phys. Res., Sect. A* **922**, 217 (2019).
- ⁵²T. Liu, W. Tang, S. Luong, and O. Fenwick, *Nanoscale* **12**, 9688 (2020).
- ⁵³C. C. Stoumpos, C. D. Malliakas, and M. G. Kanatzidis, *Inorg. Chem.* **52**, 9019 (2013).
- ⁵⁴Y. Lin, Y. Bai, Y. Fang, Q. Wang, Y. Deng, and J. Huang, *ACS Energy Lett.* **2**, 1571 (2017).
- ⁵⁵T. Niu, H. Ren, B. Wu, Y. Xia, X. Xie, Y. Yang, X. Gao, Y. Chen, and W. Huang, *J. Phys. Chem. Lett.* **10**, 2349 (2019).
- ⁵⁶G. E. Stillman, C. M. Wolfe, and J. O. Dimmock, *J. Phys. Chem. Solids* **31**, 1199 (1970).
- ⁵⁷T. Kimura, K. Matsumori, K. Oto, Y. Kanemitsu, and Y. Yamada, *Appl. Phys. Express* **14**, 041009 (2021).
- ⁵⁸H. Yücel, Ö. Birgül, E. S. R. A. Uyar, and Ş. Çubukçu, *Nucl. Eng. Technol.* **51**, 731 (2019).
- ⁵⁹P. J. Sellin and J. Vaitkus, *Nucl. Instrum. Methods Phys. Res., Sect. A* **557**, 479 (2006).
- ⁶⁰J. M. Frost, *Phys. Rev. B* **96**, 195202 (2017).
- ⁶¹K. Miyata, D. Meggiolaro, M. Tuan Trinh, P. P. Joshi, E. Mosconi, S. C. Jones, F. De Angelis, and X. Y. Zhu, *Sci. Adv.* **3**, e1701217 (2017).
- ⁶²O. Gunawan, S. R. Pae, D. M. Bishop, Y. Virgus, J. H. Noh, N. J. Jeon, Y. S. Lee, X. Shao, T. Todorov, D. B. Mitzi, and B. Shin, *Nature* **575**, 151 (2019).
- ⁶³Y. Li, C. Li, H. Yu, B. Yuan, F. Xu, H. Wei, and B. Cao, *Front. Chem.* **8**, 754 (2020).
- ⁶⁴D. Ju, X. Jiang, H. Xiao, X. Chen, X. Hu, and X. Tao, *J. Mater. Chem. A* **6**, 20753 (2018).
- ⁶⁵S. Rong, Y. Xiao, J. Jiang, Q. Zeng, and Y. Li, *J. Phys. Chem. C* **124**, 8992 (2020).
- ⁶⁶G. Maculan, A. D. Sheikh, A. L. Abdelhady, M. I. Saidaminov, M. A. Haque, B. Murali, E. Alarousu, O. F. Mohammed, T. Wu, and O. M. Bakr, *J. Phys. Chem. Lett.* **6**, 3781 (2015).
- ⁶⁷M. Ng and J. E. Halpert, *RSC Adv.* **10**, 3832 (2020).
- ⁶⁸Y. Feng, L. Pan, H. Wei, Y. Liu, Z. Ni, J. Zhao, P. N. Rudd, L. R. Cao, and J. Huang, *J. Mater. Chem. C* **8**, 11360 (2020).
- ⁶⁹B. Bin Zhang, F. Wang, H. Zhang, B. Xiao, Q. Sun, J. Guo, A. Ben Hafsia, A. Shao, Y. Xu, and J. Zhou, *Appl. Phys. Lett.* **116**, 063505 (2020).
- ⁷⁰Y. He, C. C. Stoumpos, I. Hadar, Z. Luo, K. M. McCall, Z. Liu, D. Y. Chung, B. W. Wessels, and M. G. Kanatzidis, *J. Am. Chem. Soc.* **143**, 2068 (2021).
- ⁷¹Y. Liu, Y. Zhang, X. Zhu, Z. Yang, W. Ke, J. Feng, X. Ren, K. Zhao, M. Liu, M. G. Kanatzidis, and S. Liu, *Sci. Adv.* **7**, eabc8844 (2021).
- ⁷²K. M. McCall, Z. Liu, G. Trimarchi, C. C. Stoumpos, W. Lin, Y. He, I. Hadar, M. G. Kanatzidis, and B. W. Wessels, *ACS Photonics* **5**, 3748 (2018).
- ⁷³W. Li, D. Xin, S. Tie, J. Ren, S. Dong, L. Lei, X. Zheng, Y. Zhao, and W. H. Zhang, *J. Phys. Chem. Lett.* **12**, 1778 (2021).
- ⁷⁴X. Zheng, W. Zhao, P. Wang, H. Tan, M. I. Saidaminov, S. Tie, L. Chen, Y. Peng, J. Long, and W. H. Zhang, *J. Energy Chem.* **49**, 299 (2020).
- ⁷⁵R. Zhuang, X. Wang, W. Ma, Y. Wu, X. Chen, L. Tang, H. Zhu, J. Liu, L. Wu, W. Zhou, X. Liu, and Y. (Michael) Yang, *Nat. Photonics* **13**, 602 (2019).
- ⁷⁶I. C. Smith, E. T. Hoke, D. Solis-Ibarra, M. D. McGehee, and H. I. Karunadasa, *Angew. Chem.-Int. Ed.* **53**, 11232 (2014).
- ⁷⁷D. A. Valverde-Chávez, C. S. Ponseca, C. Stoumpos, A. Yartsev, M. G. Kanatzidis, V. Sundström, and D. G. Cooke, in *CLEO Science and Innovations, CLEO-SI 2015*, [Optical Society of America (OSA), 2015], p. 2267.
- ⁷⁸O. E. Semonin, G. A. Elbaz, D. B. Straus, T. D. Hull, D. W. Paley, A. M. Van Der Zande, J. C. Hone, I. Kyimissis, C. R. Kagan, X. Roy, and J. S. Owen, *J. Phys. Chem. Lett.* **7**, 3510 (2016).
- ⁷⁹Y. S. Handayani, E. D. Indari, R. Hidayat, Y. Othsubo, and S. I. Kimura, *Mater. Res. Express* **6**, 084009 (2019).
- ⁸⁰C. Wu, D. Guo, P. Li, S. Wang, A. Liu, and F. Wu, *Phys. Chem. Chem. Phys.* **22**, 3105 (2020).
- ⁸¹A. Yangui, R. Rocanova, T. M. Mcwhorter, Y. Wu, M. H. Du, and B. Saparov, *Chem. Mater.* **31**, 2983 (2019).
- ⁸²D. B. Mitzi, K. Chondroudis, and C. R. Kagan, *Inorg. Chem.* **38**, 6246 (1999).
- ⁸³M. G. Ju, J. Dai, L. Ma, Y. Zhou, W. Liang, and X. C. Zeng, *J. Mater. Chem. A* **7**, 16742 (2019).
- ⁸⁴Y. Zhang, M. Sun, N. Zhou, B. Huang, and H. Zhou, *J. Phys. Chem. Lett.* **11**, 7610 (2020).
- ⁸⁵C. Motta, F. El-Mellouhi, and S. Sanvito, *Sci. Rep.* **5**, 12746 (2015).
- ⁸⁶T. Zhao, W. Shi, J. Xi, D. Wang, and Z. Shuai, *Sci. Rep.* **7**, 1 (2016).
- ⁸⁷S. Poncé, M. Schlipf, and F. Giustino, *ACS Energy Lett.* **4**, 456 (2019).